Published in final edited form as:

Nat Neurosci. 2013 December ; 16(12): 1794–1801. doi:10.1038/nn.3575.

Betaine acts on a ligand-gated ion channel in the nervous system of the nematode *C. elegans*

Aude S. Peden[1], **Patrick Mac**[1,*], **You-Jun Fei**[2,*], **Cecilia Castro**[3,4], **Guoliang Jiang**[2], **Kenneth J. Murfitt**[3,5], **Eric A. Miska**[3,5], **Julian L. Griffin**[3,4,6], **Vadivel Ganapathy**[2], and **Erik M. Jorgensen**[1,7]

[1]Howard Hughes Medical Institute, Department of Biology, University of Utah, Salt Lake City, UT 84112, USA

[2]Departments of Biochemistry and Molecular Biology, Georgia Regents University, Augusta, GA USA 30912, USA

[3]Department of Biochemistry, University of Cambridge, Tennis Court Rd, Cambridge CB2 1GA, UK

[4]Cambridge Systems Biology Centre, University of Cambridge, 80 Tennis Court Road, Cambridge, CB2 1GA, UK

[5]Wellcome Trust Cancer Research UK Gurdon Institute, University of Cambridge, The Henry Wellcome Building of Cancer and Developmental Biology, Tennis Court Rd, Cambridge CB2 1QN, UK

[6]The Medical Research Council Human Nutrition Research, Elsie Widdowson Laboratory, Fulborn Road, Cambridge, CB1 9NL, UK

Abstract

Prior to the advent of synthetic nematocides, natural products such as seaweed were used to control nematode infestations. The nematocidal agent in seaweed is betaine, an amino acid that functions as an osmolyte and methyl donor. However, the molecular mechanisms of betaine toxicity are unknown. Here, we identify the betaine transporter SNF-3 and a betaine receptor ACR-23 in the nematode *C. elegans*. Mutating *snf-3* in a sensitized background causes the animals to be hypercontracted and paralyzed, presumably because of excess extracellular betaine. These behavioral defects are suppressed by mutations in *acr-23*, which encodes a ligand-gated cation channel of the cys-loop family. ACR-23 is activated by betaine and functions in the

[7]Corresponding author: Erik M. Jorgensen, (801) 585-3517 (phone), (801) 585-3517 (fax), jorgensen@biology.utah.edu.
*contributed equally to this work

Author Contributions

A.S.P. designed and performed genetics screens, behavior analyses and wrote the paper. Y.J.F., G.J. and V.G. designed and performed the physiological analyses of the betaine transporter. P.M. performed the physiological analyses of the betaine receptor. J.L.G and C.C. measured betaine concentrations in the worm using NMR spectroscopy. E.A.M. and K.J.M. helped J.L.G with nematode cultures. E.M.J. provided guidance and edited the paper.

Competing financial interests

The authors declare no competing financial interests.

mechanosensory neurons to maintain basal levels of locomotion. However, overactivation of the receptor by excess betaine or by the allosteric modulator monepantel causes hypercontraction and death of the nematode. Thus, monepantel targets a betaine signaling pathway in nematodes.

Keywords

betaine receptor; SNF-3; betaine transporter; ACR-23; phospholipase Cβ; egl-8; *C. elegans*

Introduction

Humans have long competed with parasitic nematodes for crops, livestock, and personal health. Early farmers dealt with nematode infestations by using natural pesticides such as wormwood, tobacco, and algae (seaweed), which contain natural phytochemicals that interfere with parasitic nematode development[1–3]. Seaweed extracts are rich in betaines (δ-aminovaleric betaine, γ-amino-butyric betaine, and glycine betaine), and direct application of individual betaines to plants suppresses nematode growth as effectively as algal extract[4].

Glycine betaine, or simply ‘betaine’, is a ubiquitous non-canonical amino acid that acts as an osmolyte or as a methyl donor. In addition to its role in metabolism, betaine may play specific roles in the mammalian nervous system. Betaine has anti-epileptic properties [5–7] and the transporter BGT-1 is localized to dendritic spines and astrocytes in the mammalian brain[8].

In nematodes betaine arrests larval development [2–4]. However, the molecular target of betaine is not known. The targets of synthetic anthelmintics are often ligand-gated ion channels. The imidazothiazoles directly activate acetylcholine–gated ion channels, which stimulates muscle contraction and paralyzes the worm[9,10]. The macrocyclic lactones open glutamate-gated chloride channels and inhibit pharyngeal pumping [11–13]. Amino-acetonitrile derivatives (AADs) are a recently discovered class of compounds that target a nematode-specific ion channel, called ACR-23 in *C. elegans*[14]. ACR-23 belongs to the nicotinic acetylcholine receptor subfamily, but its homolog in parasitic nematodes, MPTL-1, is not gated by acetylcholine or choline[15]. The endogenous ligand and biological function of ACR-23 remain to be characterized.

In this manuscript, we study the role of betaine in the nematode *C. elegans*, and demonstrate that ACR-23 is a betaine receptor. First, we characterize the betaine transporter SNF-3 and show that mutations in this transporter are subviable in a sensitized background lacking phospholipase Cβ. Second, we demonstrate that mutations in *acr-23* suppress this lethality, suggesting that excess betaine is acting via ACR-23. Third, we demonstrate that ACR-23 is gated by betaine and potentiated by the AAD monepantel. Thus, ancient and modern anthelmintics act on the same target: a betaine-activated ion channel that is only found in nematodes.

Results

An enhancer screen identifies a betaine transporter

We were able to identify the betaine pathway inadvertently while studying phospholipase Cβ function. In the nematode *C. elegans*, mutants lacking the only phospholipase Cβ gene (*egl-8*) exhibit subtle behavioral defects in locomotion and egg-laying, in contrast to the near lethal phenotype of mutants lacking Gαq, the upstream activator of phospholipase Cβ [16,17]. This modest loss-of-function phenotype of *egl-8* suggests the existence of parallel pathways to inositol signaling that modulate locomotion. To uncover these pathways, we performed an F_2 enhancer screen in an *egl-8* mutant background. We screened 1669 haploid genomes and identified a single mutation that caused a synthetic phenotype in the presence of an *egl-8* mutation. Mapping, rescue and sequencing experiments demonstrated that the enhancer was an allele of the *snf-3* gene (*sodium neurotransmitter symporter family-3*, Supplementary Fig. S1a). The *snf-3 egl-8* double mutants exhibit severe synthetic phenotypes (Fig. 1a–d): the strain is subviable, uncoordinated, and dumpy. The dumpy phenotype is caused by hypercontraction of the muscle since it can be suppressed by mutations in the contractile apparatus *unc-22* (twitchin) and *unc-54* (myosin) (data not shown)[9]. The hypercontracted phenotype of *snf-3 egl-8* double mutants is fully synthetic: neither single mutant is hypercontracted (*snf-3 egl-8* vs *egl-8* in Fig. 1a–b, and *snf-3* in Supplementary Fig. S1c). The uncoordinated phenotype is also more severe than that of either single mutant (Fig. 1c–d). Multiple allelic combinations exhibit the same synthetic hypercontracted phenotype (data not shown), demonstrating that the phenotypes are not due to background mutations.

snf-3 encodes a neurotransmitter transporter of the solute carrier 6 (SLC6) gene family. Members of this transporter family clear neurotransmitters from the synaptic cleft, including the neurotransmitters serotonin, dopamine, norepinephrine, GABA and glycine. SNF-3 is orthologous to the vertebrate betaine/GABA transporter (BGT1 or SLC6A12). Although we do not fully understand the genetic interaction between the betaine transporter and PLCβ, the synthetic phenotype provided a selection to identify the betaine receptor.

Hypercontraction in *snf-3 egl-8* is mediated by *acr-23*

Mutations in SLC6 transporters often result in constitutive signaling because the neurotransmitter cannot be cleared from the synaptic cleft[18,19]. For example, mice lacking the dopamine transporter are hyperactive[20], while worms lacking the same gene have defects in their locomotory behaviors[21,22]. These defects are consistent with the role of dopamine in the control of locomotion.

To determine whether the phenotype of *snf-3 egl-8* mutants was caused by constitutive betaine signaling, we screened for suppressors of the *snf-3* synthetic phenotype. Specifically, we mutagenized *snf-3 egl-8* double mutants with ENU and screened for suppressors of the hypercontracted phenotype (Fig. 1e, screen 2). We screened 37,000 haploid genomes and obtained 35 suppressors. The phenotypes of the triple mutants fall into three broad classes: those that resemble *egl-8* single mutants (*snf-3* specific suppressors), those that resemble *snf-3* mutants (*egl-8* specific suppressors) and those with novel phenotypes. The strongest *snf-3*-specific suppressor was the mutation *ox429*. We identified the suppressor mutation by

genome resequencing and by transgenic rescue. o*x429* is an allele of the gene *acr-23* (*acetylcholine receptor like-23*) (Supplementary Fig. S2a). *acr-23* encodes a nematode-specific ligand-gated channel subunit and is predicted to function as a cation channel based on its sequence homology to acetylcholine receptors (Supplementary Fig. S2c). The only known function of ACR-23 is that it imparts sensitivity to the new class of anthelmintic drugs known as AADs. Genetic screens for AAD-resistance in *C. elegans* identified 27 independent mutations in a single target, *acr-23*[14] and mutations in related receptor subunits within the same subfamily do not confer resistance to AAD[23].

acr-23(ox429) fully suppresses the hypercontracted (Fig. 1f) and uncoordinated phenotypes (Fig 1g) of the *snf-3 egl-8* double mutants. For example, the double mutants are completely paralyzed in liquid (Fig. 1g, 0 % of wild-type rate), whereas the *snf-3 egl-8 acr-23* triple mutants thrash actively (Fig. 1g, 45% of wild-type rate). A deletion allele *acr-23*(*ok2804*) also suppresses the double mutants (Fig. 1f–g). The triple mutants still exhibit *egl-8* phenotypes including lethargy (Fig. 1g), constipation (data not shown), and a mild egg-laying defect (data not shown), suggesting that *acr-23* mutations specifically suppress *snf-3*, but not *egl-8* pathways.

SNF-3 is a Na^+/Cl^--dependent betaine transporter

The vertebrate ortholog of SNF-3, betaine/GABA transporter 1 (BGT1 or SLC6A12) has two substrates, betaine and GABA. However, it has a higher affinity for GABA (K_m= 93 μM) than betaine (K_m= 398 μM)[24,25]. By contrast, we find that SNF-3 transports betaine but not GABA. Betaine is a noncanonical amino acid that is present in all organisms (Fig. 2a). It acts as an osmolyte to maintain cell volume during stress[26] and as a methyl donor in the conversion of homocysteine to methionine. Betaine is acquired either by dietary uptake using a plasma membrane transporter or is generated as an oxidation product of choline[27]. Ultimately, betaine is metabolized to glycine.

To rapidly screen for the relevant substrate, we expressed SNF-3 in *Xenopus* oocytes and applied potential transport molecules. Because SLC6 transporters co-transport ions along with substrate molecules, they are electrogenic. We tested candidate substrates and found that only betaine induced a specific current (Supplementary Fig. S3a). GABA, the betaine metabolites dimethyl-glycine, N-methylglycine, glycine and other related compounds, are not substrates of the SNF-3 transporter.

To characterize the transport kinetics of SNF-3, we measured the accumulation of radio-labeled betaine in Human Retinal Pigment Epithelial (HRPE) cells, which do not express an endogenous betaine transporter. The expression of SNF-3 increased betaine uptake greater than 100-fold (108 ± 3 pmol/10^6 cells/min) over control cells (0.8 ± 0.1 pmol/10^6 cells/min). SNF-3-mediated transport was saturable with a K_m of 320 ± 50 μM (Fig. 2b); this value is similar to the affinity of BGT-1 for betaine (398 μM)[24]. As expected for protein-mediated transport, activity is saturable over a range of concentrations (Fig. 2b and Supplementary Fig. S3b) and voltages (Supplementary Fig. S3c). Like other SLC6 transporters, SNF-3 requires sodium and chloride to move substrates into cells against their chemical gradient. The absence of sodium (in NMDG chloride solution) or the absence of chloride (sodium gluconate solution) abolished betaine uptake (Fig. 2c and Supplementary Fig. S3d), and

transport is voltage-dependent (Supplementary Fig. S3e). The Michaelis constant of SNF-3 for sodium ($K_{0.5}^{NA}$) was 37 ± 1 mM with a Hill coefficient of 2.2 ± 0.1 (Supplementary Fig. S3f), and the corresponding value for chloride ($K_{0.5}^{Cl}$) was 12 ± 1 mM with a Hill coefficient of 1.0 ± 0.1 (Supplementary Fig. S3g). Thus, these data demonstrate that SNF-3 functions as a betaine transporter with a unidirectional influx of 1 betaine: 2 Na^+: 1 Cl^- per transport cycle.

In contrast to BGT1, SNF-3 does not transport GABA in our biochemical assays, and this lack of GABA transport activity has also been demonstrated functionally. In the nematode, the GABA transporter is encoded by *snf-11*[28]. Overexpression of the SNF-3 transporter was unable to compensate for the absence of the GABA transporter SNF-11 even when overexpressed under the *snf-11* promoter, indicating that SNF-3 cannot transport GABA *in vivo* [28]. The presence of a dedicated transporter suggests that betaine may play a specific role in cell signaling.

SNF-3 is required for betaine clearance

Members of the SLC6 transporter family clear neurotransmitters from synapses and the extrasynaptic space, and thereby limit their activity. To determine where SNF-3 functions, we examined *snf-3* expression using a functional SNF-3::GFP transgene (Supplementary Fig. S1b). Transgenic worms displayed strong expression in the excretory canal, tail hypodermal cells, epidermis, and vulval epithelia cells (Fig. 3a). SNF-3 was also expressed in some neurons, including the excretory canal-associated neuron (CAN, Fig. 3a), and some sensory neurons in the head including ILs, OLs, ADE and AQR (Supplementary Fig. 2d–e). We were able to rescue the hypercontraction and the locomotory phenotypes of *snf-3 egl-8* double mutants by expressing wild-type SNF-3 using the native *snf-3* promoter or using tissue-specific promoters for the excretory canal or skin (*Pglt-3* and P*pdi-2*, respectively; Fig. 3b). Interestingly, expressing SNF-3 in tissues that do not normally express the gene, such as the intestine, chemosensory neurons or acetylcholine motor neurons, also rescued the hypercontracted phenotype (Fig. 3b). Rescue requires expression during larval development: expression of SNF-3 in the intestine during larval development (P*vha-6*), but not in the adult (P*vit-2;* Fig. 3b) rescued the hypercontracted phenotype. This stage-dependent rescue is consistent with the retarded larval development of *snf-3* mutants (Supplementary Fig. S2e). The non-cell autonomous rescue of the *snf-3 egl-8* phenotypes suggests that the hypercontracted and locomotory phenotypes are caused by a lack of betaine clearance; presumably any tissue – not just the epidermis and excretory canal – can remove the excess betaine.

In contrast to *snf-3*, the phospholipase Cβ gene *egl-8* was required in the nervous system, but not epidermis (Fig. 3c). Further analyses of EGL-8 revealed that the synthetic hypercontraction is caused by a defect in acetylcholine neurons (P*unc-17*). Expression in sensory neurons (data not shown), or ventral cord motor neurons (data not shown) did not rescue the double-mutant phenotypes. Thus, the functional requirements for EGL-8 and SNF-3 are in separate tissues: the transporter SNF-3 functions primarily in the epidermis to clear betaine from the extracellular space, whereas EGL-8 is required in the nervous system to modulate neuronal activity.

Exogenous betaine paralyzes *snf-3* mutants

These data suggest that the phenotypes caused by *snf-3* mutants are due to excess betaine in the extracellular space. If true, then high levels of exogenous betaine should mimic *snf-3* phenotypes. We grew *C. elegans* on different concentrations of betaine and tested their locomotion in liquid. Wild-type worms were not affected by 50 mM betaine (Fig. 3d). *egl-8* mutants were hypersensitive to 50 mM betaine and became sluggish in liquid, but they did not become hypercontracted. *snf-3* mutants were strongly hypersensitive to 50 mM betaine and were paralyzed in liquid. The toxic effect of betaine is mediated by ACR-23 since *snf-3 acr-23* double mutants were resistant to exogenous betaine (Fig. 3d). Wild-type animals grown at a higher concentration of betaine (250 mM) exhibited slowed swimming in the presence of betaine (Fig. 3e no array), whereas animals overexpressing the SNF-3 transporter were resistant to 250 mM betaine (Fig. 3e). These data suggest that excess betaine suppresses locomotion and that the SNF-3 betaine transporter clears betaine from the extracellular space.

snf-3 mutants exhibit locomotory phenotypes even if excess betaine is not applied (Fig. 1c–d), suggesting that betaine may already be present in worms. To determine betaine levels in *C. elegans*, we performed proton-NMR spectroscopic analysis on the worm metabolome. Betaine was present in extracts of worms at 7.0 ± 1.0 μM/mg of dry pellet (Fig. 3f), whereas the concentrations of GABA and acetylcholine were below detection (data not shown). Total betaine content did not change in *snf-3* mutants but a redistribution to the extracellular space would not be detectable in assays of whole worms. Interestingly, concentrations of the metabolites choline and glycine were higher in *snf-3* mutants (Fig. 3f). Levels of betaine in *C. elegans* are controlled in part by diet[29]. To confirm that our *E. coli* strains released betaine in the media, we measured the concentration of betaine in the media. We found that the bacterial media contained betaine at 2.3 ± 0.5 mM/ml, demonstrating that betaine is readily available from food.

ACR-23 forms a homomeric betaine receptor

To test whether betaine acts directly on the ACR-23 receptor, we expressed ACR-23 in *Xenopus* oocytes and examined its response to various ligands. ACR-23 forms an ion channel that is activated by betaine, but not by acetylcholine, choline, glycine, or GABA (Fig. 4a). The sensitivity of ACR-23 for betaine is relatively weak; the EC_{50} for betaine is 1.4 mM with a Hill coefficient of 1.2 ± 0.1 (Fig. 4b–c) compared to an EC_{50} of 40 μM for GABA receptors that function at the *C. elegans* neuromuscular junction[30]. Although we could not confirm the EC_{50} by recording from larval muscles *in vivo*, the sensitivity of the channel to betaine is consistent with the high K_m of the betaine transporter (~0.3 mM) and the concentrations of betaine found in extracellular space (~0.2 mM in mammals)[24].

ACR-23 is likely to be a non-selective monovalent cation channel. Like other cation channels, ACR-23 lacks a proline at the -2’ position and has a glutamate at the -1’ position of the TM2 pore-forming helix[31] (Supplementary Fig. S2c). Betaine-induced inward currents reverse at −9.4 ± 0.9 mV (Fig. 4d), which is consistent with a non-selective cation channel. To demonstrate cation permeability, we replaced Na^+ in the extracellular solution with the large impermeant cation N-methyl-D-glucamine (NMDG). NMDG largely

abolished betaine-evoked inward currents and shifted the reversal potential to −42.8 ± 5.6 mV, indicating that monovalent cations contribute substantially to the ACR-23 current (Fig. 4d). To determine whether the ACR-23 channel is permeable to K^+ ions, we replaced external NaCl with KCl. These conditions did not cause any shift in the reversal potential (ΔE_{rev}= 0.6 ± 0.7 mV, Fig. 4e), indicating that the channel is also permeable to K^+ ions and exhibits no selectivity between Na^+ and K^+ (P_{Na}/P_K = 1.0). Two experiments demonstrate that ACR-23 exhibits little or no divalent cation permeability. First, we tested whether betaine-evoked currents could activate the endogenous Ca^{2+}-activated chloride channels in *Xenopus* oocytes, which can be activated by calcium but not barium influx through calcium-permeable ion channels[32]. However, replacement of extracellular Ca^{2+} with Ba^{2+} did not alter betaine-evoked currents in oocytes (data not shown). Second, increasing the concentration of Ba^{2+} ten-fold failed to elicit a significant shift in betaine-evoked reversal potential (ΔE_{rev}= 1.1 ± 1.1 mV, Fig. 4f). Thus, ACR-23 forms a homomeric betaine-gated ion channel that is non-selective for monovalent cations.

ACR-23 was first isolated as the target of the novel class of anthelmintic drugs called amino-acetonitrile derivatives (AADs), commercially available as Zolvix containing the AAD monepantel[14]. However, the pharmacological effects of this drug on the ACR-23 receptor have never been tested because the endogenous ligand of ACR-23 was not known[15]. To determine the effects of monepantel on ACR-23, we applied 300 pM monepantel (diluted Zolvix) to ACR-23-expressing oocytes. Monepantel did not elicit any current by itself, but rather potentiated betaine-induced currents (Fig. 4g). Recently it was observed that one thousand-fold higher concentrations of monepantel (300 nM) can act as an agonist of ACR-23[33]. At 300pM monepantel does not activate the ion channel, and has no effect on the size of the initial betaine-induced current, however, it blocks the desensitization of the ACR-23 receptor (Fig. 4g). Sixty seconds after the initial application of betaine, the current amplitude was 5.3 ± 0.9 times larger in the presence of monepantel than in its absence. Thus, monepantel functions as a positive allosteric modulator of betaine gating. Allosteric modulators, such as benzodiazepines and barbiturates that positively enhance GABA transmission, alter the response of the receptor to its natural ligand without competing for the binding site.

ACR-23 acts in the nervous system to regulate locomotion

To determine where ACR-23 functions during locomotion, we characterized the expression pattern of the *acr-23* gene using transcriptional mCherry reporter constructs (Fig. 5a and Supplementary Fig. S2b). *acr-23* is expressed strongly in the six mechanosensory neurons, multiple interneurons, and in body muscles. Muscle expression is higher in larvae and weak in adults. Expression of *acr-23* in the larval body muscles is consistent with the hypercontraction phenotype observed in *snf-3 egl-8* double mutants.

The lack of expression in motor neurons was surprising because mutants lacking *acr-23* (Supplementary Fig. S1c) exhibit mild yet significant swimming defects (Fig. 1g), are lethargic when crawling on an agar plate (Fig. 5b,c) and their movement is interrupted by frequent pauses. *snf-3* mutants and *snf-3 acr-23* double mutants are equally sluggish (Fig. 1g

and Fig. 5b–c), suggesting that the effect of betaine on locomotion is mediated by different receptors.

To determine where ACR-23 functions during locomotion, we rescued the mutant using tissue-specific promoters. Expression in the nervous system rescued the locomotory phenotypes of *acr-23* mutants (Fig. 5d). Expression in the mechanosensory neurons also partially restored motor activity (Fig. 5d), consistent with the known role for these cells in controlling basal levels of locomotion[34]. Thus, like *egl-8*, *acr-23* is also required in the nervous system. These data suggest that phospholipase Cβ is limiting ACR-23 function in the nervous system, either directly or indirectly.

Gain-of-function ACR-23 resembles *snf-3 egl-8* double mutants

Together these data suggest that an increase in betaine levels in the *snf-3 egl-8* double mutants inappropriately activates ACR-23 and leads to hypercontraction. To demonstrate that increased current via ACR-23 alone was capable of generating the hypercontracted phenotype, we generated an ACR-23 receptor with higher ligand sensitivity. The second transmembrane domain forms the pore in ligand-gated ion channels and the residues are numbered 0' to 19' by convention[35]. Mutations at the 13' position of the pore are known to increase the ligand sensitivity and conductance of cys-loop ion channels, probably by affecting transitions to the open state[31]. We engineered a variant at the 13' position, ACR-23(I301N), based on known gain-of-function mutations in a related receptors[36] (Supplementary Fig. S2c). Similar to other receptors[31], ACR-23 (I301N) was more sensitive to betaine and the channel desensitized less than the wild-type receptor (Fig. 4c). The EC_{50} for the receptor decreased 8-fold from 1400 μM to 166 μM (Fig. 4c).

This hypersensitive variant of ACR-23 in transgenic animals recapitulated the *snf-3 egl-8* double mutant phenotype. Most ACR-23(I301N) transgenic worms died during larval development. Those that escaped lethality and reached adulthood were severely hypercontracted (Supplementary Fig. S2d and Fig. 5e) and uncoordinated (Fig. 5f), closely resembling the phenotype of *snf-3 egl-8* mutants. We also evaluated the tissue-specific effects of the gain-of-function ACR-23 (I301N) mutation. Expressing ACR-23 (I301N) in body muscles alone generated hypercontracted animals that only exhibited modest locomotion defects (Fig. 5e–f and Supplementary Fig. S2e). Conversely, expression of ACR-23(I301N) in the mechanosensory neurons resulted in morphologically wild-type animals that exhibited uncoordinated thrashing in liquid (Fig. 5e–f and Supplementary Fig. S2d). These data are consistent with ACR-23 acting in part via the nematode somatosensory circuit that modulates locomotion.

Discussion

Using two forward genetic screens, we uncovered the molecular pathway that leads to betaine toxicity in nematodes. ACR-23 is a betaine-gated cation channel expressed in body muscle and neurons. The betaine transporter SNF-3 removes betaine from the extracellular space (Supplementary Fig. 4). In the absence of *snf-3* betaine can accumulate in the extracellular space, and *snf-3* mutants exhibit subtle locomotory phenotypes. These phenotypes curiously are exacerbated by mutations in phospholipase Cβ. In the *snf-3 egl-8*

double mutant, constitutive activation of ACR-23 causes hypercontraction, paralysis and sometimes death, due to a combination of effects on the nervous system and muscle. Why phospholipase Cβ mutations are synthetic with mutations in the transporter is not clear; however, one possibility is that phospholipase Cβ is required to downregulate ACR-23 itself or the activity of the neurons in which it functions. Thus, the elimination of the receptor by mutation restores muscle function and locomotion, reversing the effect of the *snf-3 egl-8* mutations.

In addition to its natural ligand betaine, ACR-23 is also the target of a novel class of anthelmintic drugs called amino-acetonitrile derivatives (AADs), commercially available as Zolvix, which contains the active compound monepantel[14]. Monepantel induces muscle hypercontraction, spasmodic pharyngeal contraction, paralysis, and death in *C. elegans*[14]. These characteristics are common to other anthelmintic drugs that activate ligand-gated ion channels in the nematode. Unlike these receptor agonists, monepantel acts as an allosteric modulator of ACR-23, potentiating betaine signaling during development and resulting in nematode death. A drawback of monepantel is that some of the genera lacking the *acr-23* gene include parasitic nematodes[23], such as *Strongyloides* and *Ascaris*, which represent a major public health concern in developing countries. Unlike *acr-23*, SNF-3 has an ortholog in most parasitic nematodes species with a sequenced genome. Thus, the betaine-SNF-3 pathway offers a unique set of targets that can be used to improve AAD efficiency, or develop new anthelmintic drugs.

What then is the normal role of betaine in the nematode? Betaine signaling is required in *C. elegans* for basal levels of locomotion: *acr-23* mutants are sluggish when crawling on agar. The effect on locomotion is mediated in part via ACR-23 receptors expressed in the mechanosensory neurons. The mechanosensory neurons innervate the locomotory command neurons to stimulate touch-induced movement as well as spontaneous levels of locomotion[37,38]. The mechanosensory neuron dendritic processes run adjacent to the epidermis and in some cases are completely embedded in the epidermal cells expressing the betaine clearance transporter SNF-3. We cannot exclude the possibility that betaine is acting as a conventional neurotransmitter, that is, that it is released onto neurons and muscles at synapses. However, it is also possible that betaine is released by the epidermis rather than by neurons. Thus, in this model the skin may both release betaine onto the mechanosensory processes and clear it from the space between the skin and dendrite, acting as both source and sink for this novel neurotransmitter.

Betaine has been shown to have anticonvulsant properties in vertebrate brain[5–7], but its mechanisms of action have not been elucidated. While *acr-23* is not conserved in the vertebrate, *snf-3* and phospholipase Cβ are conserved and expressed in the vertebrate nervous system. The mammalian nervous system contains many uncharacterized ligand-gated ion channels and G-protein coupled receptors. Some of these could potentially mediate betaine anticonvulsive properties.

Methods

Genetic Screens

Enhancer screen—We mutagenized EG4094 *egl-8(sa47) V; oxEx771[B0348 egl-8(+); rol-6(sd);* P*myo-2::GFP]* with 20nM ENU. B0348 is a cosmid that rescues *egl-8*, the gene encoding phospholipase-C β. We singled individual F_1 and F_2 offspring carrying the *plcβ* rescuing extrachromosomal array, *oxEx771[B0348 (egl-8$^+$; rol-6(sd);* P*myo-2::GFP]*. We screened F_3 offspring for the presence of an enhancer by looking for novel phenotypes in non-GFP expressing siblings (*plcβ* mutant background), not observed in GFP expressing siblings (*plcβ* rescued). We screened 1669 haploid genomes and isolated *snf-3(ox354)* from this screen.

We mapped *snf-3(ox354)* to the left arm of chromosome II using single nucleotide polymorphism mapping[39]. The region was further narrowed by rescuing *snf-3* using standard microinjection transgenic techniques[40]. *snf-3(ox354)* was rescued by injecting *snf-3(ox354) egl-8(sa47)* animals with a pool of cosmids F45D11, M01D1 and C07D2 along with 2 ng μl^{-1} P*myo-2::GFP* co-injection marker. Each cosmid was injected at 20 ng μl^{-1}. Cosmid C07D2 alone was sufficient to rescue the *snf-3(ox354)* enhancer defects. We were able to rescue *snf-3(ox354)* by injecting 4 overlapping PCR fragments from wild-type genomic DNA of the T13B5.1 gene. To identify the molecular lesion in *snf-3(ox354)*, we sequenced *snf-3* PCR fragments generated from *snf-3(ox354) egl-8(sa47)* double mutants animals.

Suppressor screen—We mutagenized EG7081 *snf-3(ox354); egl-8(sa47)* with 20 nM ENU. We screened the F_2 progeny for non-hypercontracted and non-uncoordinated animals. We screened a total of 37,000 haploid genomes. We isolated *acr-23(ox429)* from this screen.

To identify the mutation *ox429*, we resequenced the genome of EG6501 *snf-3(ox354) egl-8(sa47) acr-23(ox429)* using an Illumina Genome Analyzer II (GAII). The molecular lesion in *acr-23(ox429)* was confirmed using traditional Sanger sequencing. To rescue *acr-23(ox429)*, we injected *snf-3 egl-8 acr-23* triple mutants (EG6501) with either 4 overlapping PCR fragments with a 1kb overlap (25ng μl^{-1} each) of *acr-23* genomic DNA or a full-length *acr-23* gene with 2 ng μl^{-1} P*myo-2::mCherry* co-injection marker. From injections of these two constructs, we obtained over 10 transgenic lines with the restoration of the hypercontracted phenotype observed in simple *snf-3 egl-8* double mutants. Most of these transgenic strains were very sick and hard to maintain. We further confirmed that *ox429* was an allele of *acr-23* by crossing a null allele of *acr-23(ok2804)* into *snf-3 egl-8* double mutants to generate *snf-3 egl-8 acr-23(ok2804)* (EG6544).

Molecular biology

snf-3—To create a full-length genomic *snf-3* DNA plasmid, we excised a 15kb genomic fragment of *snf-3* from C07D2 using StuI and restriction digest and ligated it into pLITMUS38 (pADA49). To generate a fluorescently tagged SNF-3, we cut the GFP with MluI from the pPD114.24 vector (Andy Fire), and ligated it into an MluI site in the largest

intron in frame with the gene to generate pADA65. The GFP tag is located in the extracellular loop between transmembrane domain 9 and 10. 30ng μl^{-1} of pADA65 was injected in *snf-3(ox354) egl-8(sa47)* along with 2 ng μl^{-1} P*myo-3::mCherry* and P*unc-122::GFP* co-injection marker. Multiple transgenic lines were obtained and they fully rescued *snf-3(ox354)* enhancer defects (strain EG4769 carries *oxEx1067*). We also tagged SNF-3 at the N-terminus by ligating P*snf-3* and the *snf-3* coding region into the GFP vector pPD117.01 (Andy Fire) to generate pADA73. 10ng μl^{-1} of pADA73 was injected into *lin-15(n765ts)* along with 2 ng μl^{-1} P*myo-3::mCherry* co-injection marker and *lin-15(+)* (pL15EK). We generated EG6888 from these injections. To visualize neurons expressing SNF-3::GFP, we subjected EG6888 to RNAi feeding plates against GFP (pPD128.110). For tissue-specific rescue, we used the MultiSite Gateway Pro 3-fragment recombination technology (Invitrogen, Grand Island, NY; catalog no.12537-023). All constructs containing a promoter were inserted into the pDONR™P4-P1 vector (slot 1). These promoters contained the initiating start codon (ATG). *snf-3* cDNA, lacking the ATG, was inserted into the pDONR™221 vector (slot 2). The C-terminal tag fluorescent protein (GFP or mCherry) followed by the 3'UTRs of *unc-54* or *let-858* gene were inserted into pDONR™P2R-P3 vector (slot 3). The final recombination product was inserted into pDEST™R4-R3 vector.

egl-8—To create rescuing constructs for *egl-8*, we used MultiSite Gateway Technology. *egl-8* cDNA without an ATG was inserted into the pDONR™221 vector (slot 2).

acr-23—To create a full-length genomic *acr-23* construct, we divided the genomic region into three fragments that were inserted into different Multisite Gateway pDONR vectors. A 2.9kb promoter and the full genomic region except for the last two exons of the gene were inserted into the pDONR™P4-P1 vector. The 4kb intron and exon 8 were inserted into the pDONR™221 vector, and the last exon and the 3'UTR (252bases) were inserted into pDONR™P2R-P3 vector. These three fragments were recombined with pDEST™R4-R3 vector to create pADA246. To create pASP268, we inserted mCherry in operon between the last exon of the gene and the 3'UTR in the pDONR™P2R-P3 vector using Gibson Assembly Cloning technology (New England Biolab, Ipswich, MA). The intergenic region of the *gdp-2 gdp-3* was used to express mCherry from an operon. All the constructs used for tissue specific rescues were created using the MultiSite Gateway Technology. An *acr-23* cDNA containing an ATG was inserted into the pDONR™221 vector. In this case, the corresponding promoters (P*myo-3*, P*rab-3* and P*mec-7*) in slot 1 lack ATG.

Confocal microscopy

We acquired images of fluorescently-tagged fusion proteins in living *C. elegans* with a 63X 1.4NA oil objective on a Pascal LSM5 confocal microscope (Carl Zeiss, Inc).

Body length assay—We selected L4 worms the day before the assay for each genotype studied. On the day of the experiment, we anesthetized adult worms with 15 mM sodium azide in M9 solution on freshly made 2% agarose pads. We used a plan-Neofluar 10x 0.3 NA objective on a Pascal LSM5 confocal microscope. The size of the worm was determined using a build-in function on the LSM5 image browser.

Behavioral assays

Growth assay—We plated 10 L4 larvae on NGM plates 12 hr before we started the experiment. We transferred the adults every 6.5 hours (at room temperature) or overnight 12 hours (at 15 °C). After the animals were transferred, we counted the number of eggs laid. We monitored hatching rate and development rate to adulthood. Adulthood was determined by the presence of a vulva. The percentage of animals was normalized to each plate.

Betaine assay—We top-spreaded NGM plates with betaine to obtain a final concentration of 50mM and 250mM. These plates were allowed to dry at room temperature for 24 hours and then seeded with the *E. coli* strain OP50. On the day of the experiment, we added 3 L4 worms to each plate. The plates were coded so the experimenter was blind to betaine concentrations and genotype of the strains. The first and second generations progeny were then tested in a thrashing assay. For the *snf-3* overexpression line (EG8093), the array *oxEx1208* was crossed out from strain EG5051 and crossed twice against N2.

Thrashing assay for locomotion—Single young adult worms were placed in a microtiter well in a 96-well plate without agar, containing 150 μl water. Assays in M9 yielded similar results (not shown). The animal was allowed to acclimate for 2 min and we counted thrashes for 60 sec. One thrash reflects the bending of the body from the midbody toward one side of the animal and back again. The value obtained is doubled to reflect the true number of bends.

Crawling assay for locomotion—We transferred well-fed young adult animals to a food-free NGM plate (100mm). Animals were allowed to acclimate for 5 minutes, then we counted the number of body bends generated by each animal every 20 seconds. Each animal was tested 4 times.

Crawling speed assay—The speed of the worm was determined using an automated worm tracking and analysis system. A single young adult animal was transferred to to a food-free NGM plate (100mm) placed on a motorized microscope stage (OptiScan™ ES111, Prior Scientific, Inc., Rockland, MA). After 1 minute acclimation period, the worm was imaged at 5 frames per second for 5 minutes using a VGA FireWire camera (XCD-V60, Sony, Tokyo, Japan) mounted on a Leica MS5 stereomicroscope (Wetzlar, Germany). A custom MATLAB program[41] (The MathWorks, Inc., Natick, MA) was used to control the camera and the motorized stage and to determine the mean locomotion speed. The speed was calculated based on the distance traveled by the worm over 5 minutes.

Statistical Analysis

Statistical analyses were performed using Kaleidagraph 3.6, and GraphPad Prism 6. All grouped data are reported as means ± s.e.m. Statistical significance between genotypes was determined using one-way ANOVA followed by Tukey post-hoc comparisons. We used two-tailed unpaired Student's t-test with Welch's correction to determine the difference between wild-type and the gain-of-function (Fig. 4c). Logarithmic normal distribution was assumed for betaine EC_{50} values, so we use the pEC_{50} values for statistical analysis. $p < 0.05$ was considered statistically significant. No statistical methods were used to

predetermine sample sizes, but our sample sizes are similar to those reported in previous publications in the field (thrash assay[42], speed[41], body bends[21], and body length[43]). Data distributions were assumed to be normal, but this was not formally tested. Data collection and analysis were not always performed blind, but we specifically state which experiments were performed blind in the method section. All the data were collected and processed side by side in a randomized manner.

SNF-3 transport assay in HRPE cells

HRPE cells were transfected using a vaccinia virus expressing SNF-3 cDNA as described previously[44,45]. HRPE cells grown in 24-well plates were infected with a recombinant vaccinia virus (VTF7–3). This virus carries the gene for T7 RNA polymerase in its genome. The virus was allowed to adsorb onto the cells for 30 min at 37°C with gentle shaking of the plate. Cells were then transfected with the plasmid DNA (empty vector pSPORT1 or SNF-3 cDNA construct) using the lipofection procedure (Invitrogen). The cells were incubated at 37 °C for 12 h and then assayed for transport activity. The uptake of [^{14}C]betaine (2.5 μM) was determined at 37 °C. In most experiments, the media was 25 mM Hepes/Tris, pH 7.5, 140 mM NaCl, 5.4 mM KCl, 1.8 mM $CaCl_2$, 0.8 mM $MgSO_4$, and 5 mM glucose. In experiments in which the cation and anion dependence of the transport process was investigated, NaCl was replaced isoosmotically by sodium gluconate or *N*-methyl-D-glucamine (NMDG) chloride. Uptake measurements were routinely made in parallel in control cells transfected with vector alone and in cells transfected with the vector-cDNA construct. The uptake activity in cDNA-transfected cells was adjusted for the endogenous activity measured in control cells to calculate the cDNA-specific activity. Experiments were performed in triplicate, and each experiment was repeated at least three times. Results are presented as means ± s.e. The kinetic parameters, Michaelis-Menten constant (K_m) and maximal velocity (V_{max}), were calculated by fitting the data to a Michaelis-Menten equation describing a single saturable transport system. Analysis was done by nonlinear regression, and the resultant values for the kinetic parameters were confirmed by linear regression.

Electrophysiological studies in *Xenopus* oocytes

SNF-3 analysis—The procedures for cRNA *in vitro* transcription, *Xenopus laevis* oocyte isolation, microinjection, superfusion, voltage clamping and data analysis have been described previously[45,46]. Briefly, the plasmid SNF-3::pSPORT1 was linearized with NotI and transcribed *in vitro* to cRNA using the mMESSAGE mMACHINE RNA transcription kit (Ambion, Austin, TX). The expression of SNF-3 was initially detected by comparing the uptake of (2.5 μM) [^{14}C]-betaine (55 mCi/mmol, American Radiolabeled Chemicals, St. Louis, MO) in water-injected oocytes versus SNF-3-injected oocytes. The electrophysiological characteristics of the heterologously expressed SNF-3 were then studied using a GeneClamp 500 (Axon Instruments). Kinetic parameters for the saturable transport of SNF-3 were calculated using the Michaelis-Menten equation. Data were analyzed by nonlinear regression and confirmed by linear regression.

ACR-23 analysis—ACR-23 analysis was performed as described previously[47]. To generate plasmid constructs for *Xenopus* oocyte expression, we subcloned full-length error-free ACR-23 cDNAs and ACR-23 gain-of-function (ACR-23(I301N)) into the pSGEM

expression vector using the SLIC cloning technique[48] to produce pADA206 and pADA278. RNAs were prepared using the T7 mMessage mMachine kit (Ambion). Capped ACR-23 (0.1–5 ng total) or ACR-23(I301N) (0.5–2.5 ng total) RNAs were injected into *Xenopus* oocytes. 1– 4 days post-injection, two-electrode voltage clamp recordings were performed. Voltage was clamped at −60 mV. The standard bath solution was Ringer's: 115 mM NaCl, 2.5 mM KCl, 1.8 mM $CaCl_2$, 10 mM Hepes, pH 7.2 (NaOH). Each oocyte was subjected to 20 s applications of agonist with 2 minutes wash between test applications. Expression of ACR-23(I301N) was very toxic to *Xenopus* oocytes. We only used healthy oocytes with low channel expression for further analysis of this receptor. Eight oocytes were used to characterize the betaine concentration-response relationship of ACR-23(I301N), but individual oocytes were not tested through the full range of active concentrations. Three oocytes were tested at 0.001– 0.003 mM, 5 were tested at 0.01– 0.3 mM, and all were tested at 1–10 mM. Curves were fit to data from the 5 oocytes with data in the linear response range to perform statistical analysis of EC_{50} values.

Ion selectivity—For voltage-ramp experiments, $CaCl_2$ was replaced by $BaCl_2$ in the extracellular solutions in order to eliminate possible contributions from the endogenous Ca^{2+}-activated chloride channel. To assay sodium permeability, we substituted 115 mM N-methyl-D-glucamine (NMDG) chloride for NaCl. Thus Na-free solution contains 115 mM NMDG, 2.5 mM KCl, 1.8 mM $BaCl_2$, and 10 mM Hepes, pH 7.2 (HCl). To compare sodium and potassium permeability, NaCl was replaced with equimolar KCl: 115 mM KCl, 2.5 mM NaCl, 1.8 mM $BaCl_2$, 10 mM Hepes, pH 7.2 (KOH). To assay barium permeability, $BaCl_2$ was increased tenfold: 115 mM NaCl, 18 mM $BaCl_2$, 2.5 mM KCl, 10 mM HEPES, pH 7.2 (NaOH). The osmolarity of each solution was adjusted to 300 mOsm with sucrose. Reversal potentials were measured using 2 s voltage ramps (−100 mV to +60 mV) during sustained betaine application. Reversal potential shifts were similar at various time points after initiating betaine perfusion. Ramps at 20 s were analyzed for the potassium substitution experiment because of changing rectification characteristics at later time points, while ramps at 60 s were used for all other analyses. An agar bridge was used to minimize changes in junction potentials when switching solutions. Small residual voltage offsets due to differing ion composition in perfusion buffers were measured relative to standard solution before each voltage ramp recording, and were subtracted from the amplifier command voltages during data analysis. Data analysis was performed using Igor software (WaveMetrix). All chemicals were purchased from Sigma Chemical Co. (St. Louis, MO).

Monepantel—Commercially available Zolvix (25 mg/ml monepantel, Novartis) was diluted in DMSO to make a 10 mM stock solution of monepantel. The stock solution was diluted in water to make a 10 μM working stock in 0.1% DMSO. Final concentrations were achieved by diluting in Ringer's to make the experimental perfusion solutions. 1 mM betaine was applied for 60 s either alone or in the presence of 0.3 nM monepantel following a 40 s pre-application of monepantel alone. All perfusion buffers were supplemented with 0.1% DMSO. Peak current magnitudes in three 10 s time windows were compared in the presence and absence of monepantel: (1) immediately after applying monepantel alone, (2) immediately after initiating betaine application, and (3) 50 s after sustained betaine application.

NMR spectroscopy

Culture of nematodes—Strain genotypes were blinded to the experimenter. Early embryos were isolated by alkaline hypochlorite treatment and plated after synchronization on NGM plates seeded with HB101 bacteria as a food source at 20 °C. For each biological replicate, ~8000 animals were harvested, washed twice with M9, twice with water and stored at −80 °C until extraction. Eight samples were grown for each strain.

Extraction procedure for metabolites—Metabolites from whole nematodes were extracted using a methanol–chloroform procedure. 600 μl of a methanol–chloroform mix (2:1 v:v) was added to the frozen nematodes. Samples were homogenised using a Polytron and sonicated for 15 min. 200 μl each of chloroform and water were added, the samples centrifuged and the aqueous layer separated from the lipid one. The procedure was repeated twice. The aqueous layer was dried overnight in an evacuated centrifuge.

Analysis of aqueous extracts—The dried extracts were rehydrated in 600 μl D_2O, containing 0.05 mM sodium-3-(tri-methylsilyl)-2,2,3,3-tetradeuteriopropionate (TSP) (Cambridge Isotope Laboratories, MA, USA) as an internal standard. The samples were analyzed using an AVANCE II+ NMR spectrometer operating at 500.13 MHz for the ^1H frequency (Bruker, Germany) using a 5 mm TXI probe. Spectra were collected using a solvent suppression pulse sequence based on a one-dimensional NOESY pulse sequence to saturate the residual ^1H water signal (relaxation delay = 2 s, t_1 increment = 3 μs, mixing time = 150 ms, solvent presaturation applied during the relaxation time and the mixing time). 196 transients were collected into 16 K data points over a spectral width of 12 ppm at 27 °C for the adult samples.

Analysis of the metabolic profile of the bacteria—400 μl of the bacteria (HB101) broth used to feed worms was mixed with 600 μl of water and centrifuged. The supernatant was collected and dried in an evacuated centrifuge. The dried samples were rehydrated in 600 μl D2O, containing 0.05 mM sodium-3-(tri-methylsilyl)-2,2,3,3-tetradeuteriopropionate (TSP) (Cambridge Isotope Laboratories, MA, USA) as an internal standard and analyzed by NMR spectroscopy in the same way as the extracts described above. 128 transients were collected for these samples.

Data processing—NMR spectra were processed using an ACD one-dimensional NMR processor (vers. 13, ACD, Toronto, Canada). Free induction decays were Fourier transformed following multiplication by a line broadening of 1 Hz, and referenced to TSP at 0.0 ppm. Spectra were phased and baseline corrected manually. Each spectrum was integrated using 0.02 ppm integral regions between 0.5 and 4.5, and 5.5–9.5 ppm. Each spectral region was normalized to a total integral value of 1000. In addition the resonances of selected metabolites (betaine, choline and glycine) were integrated using the software package Chenomx vs. 7.1. The integrals were normalized to total pellet dry weight.

Multivariate analysis of metabolic profiles: Each set of metabolic profiles obtained were analysed by multivariate analysis. Datasets were imported into SIMCA-P 12.0 (Umetrics, Umeå, Sweden) for processing using PCA and PLS-DA (a regression extension of PCA

used for supervised classification). Proton NMR data were Pareto scaled, in which each variable was centered and multiplied by $1/(S_k)^{1/2}$ where S_k is the standard deviation of the variable.

Transgenic worms

The plasmids used in this study were generated using standard molecular biology techniques and Gateway technology (Invitrogen). All transgenic strains were generated by standard microinjection techniques[40].

Strains

The Bristol N2 strain was used as the wild type; worms were raised at room temperature (22 °C) on NGM plates seeded with OP50 *E. coli*. All other strains generated for this work are listed in Table 1.

Supplementary Material

Refer to Web version on PubMed Central for supplementary material.

Acknowledgements

We thank the following people for their help. Erik M. Peden for comments and input on the manuscript; Jim Rand and Greg Mullen and the Caenorhabditis Genetics Center for providing strains, M. Wayne Davis and Colin Thacker for Illumina sequencing analysis, Andy Fire for providing the GFP expression vectors, Zhao-Wen Wang for the worm tracker, Hsiao-Fen Han, Jann W. Gardner and Dane Maxfield for help with locomotion assays. We also thank Robin Gasser for his generous gift of Zolvix. This work was supported by grants from the National Institutes of Health, AG22468 (YJF), NS034307 (EMJ) and NRSA F32GM084596 (ASP); and the National Science Foundation grant IOS-0920069 (EMJ). EMJ is an investigator of the Howard Hughes Medical Institute.

Reference

1. Morgan K, Tarjan A. Management of Sting Nematode on Centipede grass with Kelp Extracts. Proceedings of the Florida State Horticultural Society Soc. 1980; 93:97–99.
2. Wu Y, Jenkins T, Blunden G, Whapham CA, Hankins SD. The role of betaines in alkaline extracts of Ascophyllum nodosum in the reduction of Meloidogyne javanica and M. incognita infestations of tomato plants. Fundamental and applied nematology. 1997; 20:99–102.
3. Whapham CA, Jenkins T, Blunden G, Hankins SD. The role of seaweed extracts, Ascophyllum nodosum, in the reduction in fecundity of Meloidogyne javanica. Fundamental and applied nematology. 1994; 17:181–183.
4. Wu Y, Jenkins T, Blunden G, von Mende N, Hankins S. Suppression of fecundity of the root-knot nematode, Meloidogyne javanica, in monoxenic cultures of Arabidopsis thaliana treated with an alkaline extract of Ascophyllum nodosum. Journal of Applied Phycology. 1998; 10:91–94.
5. Ghoz EH, Freed WJ. Effects of betaine on seizures in the rat. Pharmacol. Biochem. Behav. 1985; 22:635–640. [PubMed: 3991772]
6. Freed WJ, Gillin JC, Wyatt RJ. Anticonvulsant properties of betaine. Epilepsia. 1979; 20:209–213. [PubMed: 446432]
7. Wuerthele SE, Yasuda RP, Freed WJ, Hoffer BJ. The effect of local application of homocysteine on neuronal activity in the central nervous system of the rat. Life Sci. 1982; 31:2683–2691. [PubMed: 6130457]
8. Zhu X-M, Ong W-Y. A light and electron microscopic study of betaine/GABA transporter distribution in the monkey cerebral neocortex and hippocampus. J. Neurocytol. 2004; 33:233–240. [PubMed: 15322381]

9. Lewis JA, Wu CH, Berg H, Levine JH. The genetics of levamisole resistance in the nematode Caenorhabditis elegans. Genetics. 1980; 95:905–928. [PubMed: 7203008]
10. Lewis JA, Wu CH, Levine JH, Berg H. Levamisole-resistant mutants of the nematode Caenorhabditis elegans appear to lack pharmacological acetylcholine receptors. Neuroscience. 1980; 5:967–989. [PubMed: 7402460]
11. Dent JA, Davis MW, Avery L. avr-15 encodes a chloride channel subunit that mediates inhibitory glutamatergic neurotransmission and ivermectin sensitivity in Caenorhabditis elegans. EMBO J. 1997; 16:5867–5879. [PubMed: 9312045]
12. Arena JP, Liu KK, Paress PS, Schaeffer JM, Cully DF. Expression of a glutamate-activated chloride current in Xenopus oocytes injected with Caenorhabditis elegans RNA: evidence for modulation by avermectin. Brain Res. Mol. Brain Res. 1992; 15:339–348. [PubMed: 1279355]
13. Cully DF, et al. Cloning of an avermectin-sensitive glutamate-gated chloride channel from Caenorhabditis elegans. Nature. 1994; 371:707–711. [PubMed: 7935817]
14. Kaminsky R, et al. A new class of anthelmintics effective against drug-resistant nematodes. Nature. 2008; 452:176–180. [PubMed: 18337814]
15. Rufener L, Baur R, Kaminsky R, Maser P, Sigel E. Monepantel allosterically activates DEG-3/DES-2 channels of the gastrointestinal nematode Haemonchus contortus. Mol Pharmacol. 2010
16. Lackner MR, Nurrish SJ, Kaplan JM. Facilitation of synaptic transmission by EGL-30 Gqalpha and EGL-8 PLCbeta: DAG binding to UNC-13 is required to stimulate acetylcholine release. Neuron. 1999; 24:335–346. [PubMed: 10571228]
17. Miller KG, Emerson MD, Rand JB. Goalpha and diacylglycerol kinase negatively regulate the Gqalpha pathway in C. elegans. Neuron. 1999; 24:323–333. [PubMed: 10571227]
18. Torres GE, Gainetdinov RR, Caron MG. Plasma membrane monoamine transporters: structure, regulation and function. Nat Rev Neurosci. 2003; 4:13–25. [PubMed: 12511858]
19. Hahn MK, Blakely RD. The Functional Impact of SLC6 Transporter Genetic Variation. Annu. Rev. Pharmacol. Toxicol. 2007; 47:401–441. [PubMed: 17067279]
20. Giros B, Jaber M, Jones SR, Wightman RM, Caron MG. Hyperlocomotion and indifference to cocaine and amphetamine in mice lacking the dopamine transporter. Nature. 1996; 379:606–612. [PubMed: 8628395]
21. Sawin ER, Ranganathan R, Horvitz HR. C. elegans Locomotory Rate Is Modulated by the Environment through a Dopaminergic Pathway and by Experience through a Serotonergic Pathway. Neuron. 2000; 26:619–631. [PubMed: 10896158]
22. McDonald PW, et al. Vigorous Motor Activity in Caenorhabditis elegans Requires Efficient Clearance of Dopamine Mediated by Synaptic Localization of the Dopamine Transporter DAT-1. J. Neurosci. 2007; 27:14216–14227. [PubMed: 18094261]
23. Rufener L, Keiser J, Kaminsky R, Mäser P, Nilsson D. Phylogenomics of ligand-gated ion channels predicts monepantel effect. PLoS Pathog. 2010; 6
24. Yamauchi A, et al. Cloning of a Na+- and Cl-dependent betaine transporter that is regulated by hypertonicity. Journal of Biological Chemistry. 1992; 267:649–652. [PubMed: 1370453]
25. Borden LA, Smith KE, Gustafson EL, Branchek TA, Weinshank RL. Cloning and expression of a betaine/GABA transporter from human brain. J. Neurochem. 1995; 64:977–984. [PubMed: 7861179]
26. Hoffmann EK, Lambert IH, Pedersen SF. Physiology of cell volume regulation in vertebrates. Physiol. Rev. 2009; 89:193–277. [PubMed: 19126758]
27. Craig SA. Betaine in human nutrition. The American Journal of Clinical Nutrition. 2004; 80:539–549. [PubMed: 15321791]
28. Mullen GP, et al. The Caenorhabditis elegans snf-11 gene encodes a sodium-dependent GABA transporter required for clearance of synaptic GABA. Mol. Biol. Cell. 2006; 17:3021–3030. [PubMed: 16641366]
29. Reinke SN, Hu X, Sykes BD, Lemire BD. Caenorhabditis elegans diet significantly affects metabolic profile, mitochondrial DNA levels, lifespan and brood size. Mol. Genet. Metab. 2010; 100:274–282. [PubMed: 20400348]

30. Bamber BA, Beg AA, Twyman RE, Jorgensen EM. The Caenorhabditis elegans unc-49 Locus Encodes Multiple Subunits of a Heteromultimeric GABA Receptor. J. Neurosci. 1999; 19:5348–5359. [PubMed: 10377345]
31. Galzi J-L, et al. Mutations in the channel domain of a neuronal nicotinic receptor convert ion selectivity from cationic to anionic. Nature. 1992; 359:500–505. [PubMed: 1383829]
32. Vernino S, Amador M, Luetje CW, Patrick J, Dani JA. Calcium modulation and high calcium permeability of neuronal nicotinic acetylcholine receptors. Neuron. 1992; 8:127–134. [PubMed: 1370370]
33. Rufener L, et al. acr-23 Encodes a Monepantel-Sensitive Channel in Caenorhabditis elegans. PLoS Pathog. 2013; 9:e1003524. [PubMed: 23950710]
34. Chalfie M, Sulston J. Developmental genetics of the mechanosensory neurons of Caenorhabditis elegans. Dev. Biol. 1981; 82:358–370. [PubMed: 7227647]
35. Keramidas A, Moorhouse AJ, Schofield PR, Barry PH. Ligand-gated ion channels: mechanisms underlying ion selectivity. Prog. Biophys. Mol. Biol. 2004; 86:161–204. [PubMed: 15288758]
36. Treinin M, Chalfie M. A mutated acetylcholine receptor subunit causes neuronal degeneration in C. elegans. Neuron. 1995; 14:871–877. [PubMed: 7718248]
37. Riddle DL, Blumenthal T, Meyer BJ, Priess JR. Mechanosensory Control of Locomotion. 1997 . At<http://www.ncbi.nlm.nih.gov/books/NBK20005/>.
38. Chalfie M, et al. The neural circuit for touch sensitivity in Caenorhabditis elegans. J. Neurosci. 1985; 5:956–964. [PubMed: 3981252]
39. Davis MW, et al. Rapid single nucleotide polymorphism mapping in C. elegans. BMC Genomics. 2005; 6:118. [PubMed: 16156901]
40. Mello CC, Kramer JM, Stinchcomb D, Ambros V. Efficient gene transfer in C.elegans: Extrachromosomal maintenance and integration of transforming sequences. EMBO Journal. 1991; 10:3959–3970. [PubMed: 1935914]
41. Chen B, et al. α-Catulin CTN-1 is required for BK channel subcellular localization in C. elegans body-wall muscle cells. EMBO J. 2010; 29:3184–3195. [PubMed: 20700105]
42. Miller KG, et al. A genetic selection for Caenorhabditis elegans synaptic transmission mutants. Proc. Natl. Acad. Sci. U.S.A. 1996; 93:12593–12598. [PubMed: 8901627]
43. Hammarlund M, Davis WS, Jorgensen EM. Mutations in β-Spectrin Disrupt Axon Outgrowth and Sarcomere Structure. J Cell Biol. 2000; 149:931–942. [PubMed: 10811832]
44. Fei YJ, Fujita T, Lapp DF, Ganapathy V, Leibach FH. Two oligopeptide transporters from Caenorhabditis elegans: molecular cloning and functional expression. Biochem J. 1998; 332:565–572. [PubMed: 9601088]
45. Jiang G, et al. A Na+/Cl- -coupled GABA transporter, GAT-1, from Caenorhabditis elegans: structural and functional features, specific expression in GABA-ergic neurons, and involvement in muscle function. J. Biol. Chem. 2005; 280:2065–2077. [PubMed: 15542610]
46. Fei Y-J, et al. Expression cloning of a mammalian proton-coupled oligopeptide transporter. Nature. 1994; 368:563–566. [PubMed: 8139693]
47. Beg AA, Jorgensen EM. EXP-1 is an excitatory GABA-gated cation channel. Nat. Neurosci. 2003; 6:1145–1152. [PubMed: 14555952]
48. Li MZ, Elledge SJ. Harnessing homologous recombination in vitro to generate recombinant DNA via SLIC. Nat. Methods. 2007; 4:251–256. [PubMed: 17293868]

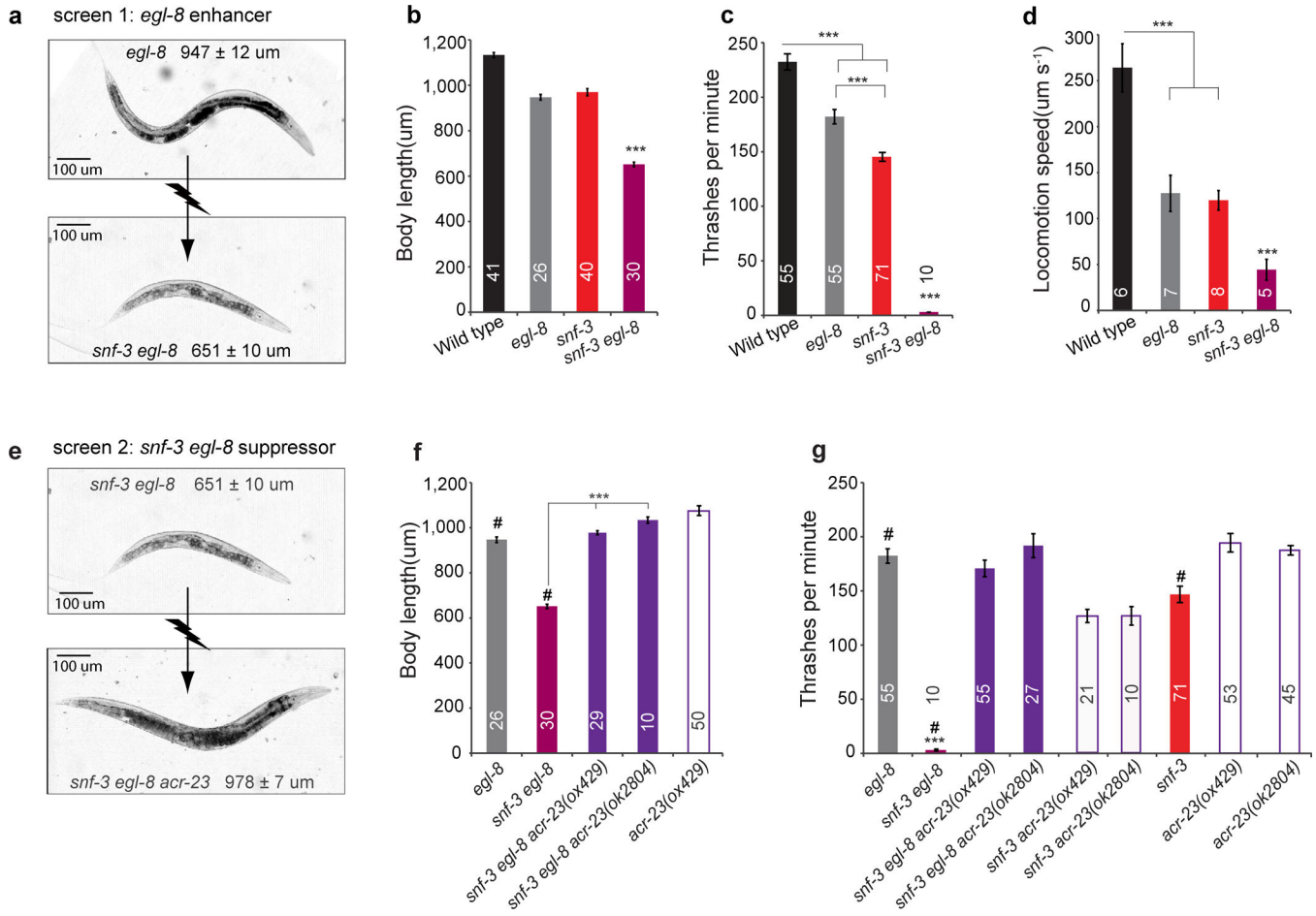

Figure 1. Two genetics screens reveal a betaine receptor

(**a**) *snf-3* was identified as an enhancer of the phosopholipase Cβ mutation *egl-8(sa47)*. Images of adult hermaphrodites of the phosopholipase Cβ mutant *egl-8(sa47)* and the *snf-3(ox354) egl-8(sa47*) double mutant that was isolated in the screen. Mean lengths of 26 (*egl-8*) and 30 (*snf-3; egl-8*) adults are shown. (**b**) Hypercontracted phenotype. Mean body length of young adult animals in micrometers ± s.e.m. *** $p< 0.001$ relative to wild type and single mutants. Genotypes are wild-type, *egl 8(sa47), snf-3(ox354),* and *snf-3(ox354) egl-8(sa47*). (**c**) Quantification of locomotion in liquid using a thrashing assay (thrashes ± s.e.m. *** $p< 0.001$). (**d**) Average locomotion speed over a 5-minute period on an agar plate without food (speed ± s.e.m. *** $p< 0.001$). Speed was determined using an automated worm tracking system. (**e**) *acr-23* was isolated as a suppressor of the *snf-3 egl-8* hypercontracted phenotype. Images of adult hermaphrodites of the *snf-3(ox354) egl-8(sa47*) double mutant ($n = 30$) and the *snf-3(ox354) egl-8(sa47*) *acr-23(ox429)* triple mutant ($n = 29$). (**f, g**) Quantification of the hypercontracted (**f**) and locomotion (**g**) phenotypes. Data represent the mean ± s.e.m. *** $p< 0.001$ compared to other mutants. For all histograms, the number of animals tested is shown inside each bar. Statistical significance was determined using one-way ANOVA followed by Tukey post-hoc comparisons. #, data are the same as Fig. 1b,c.

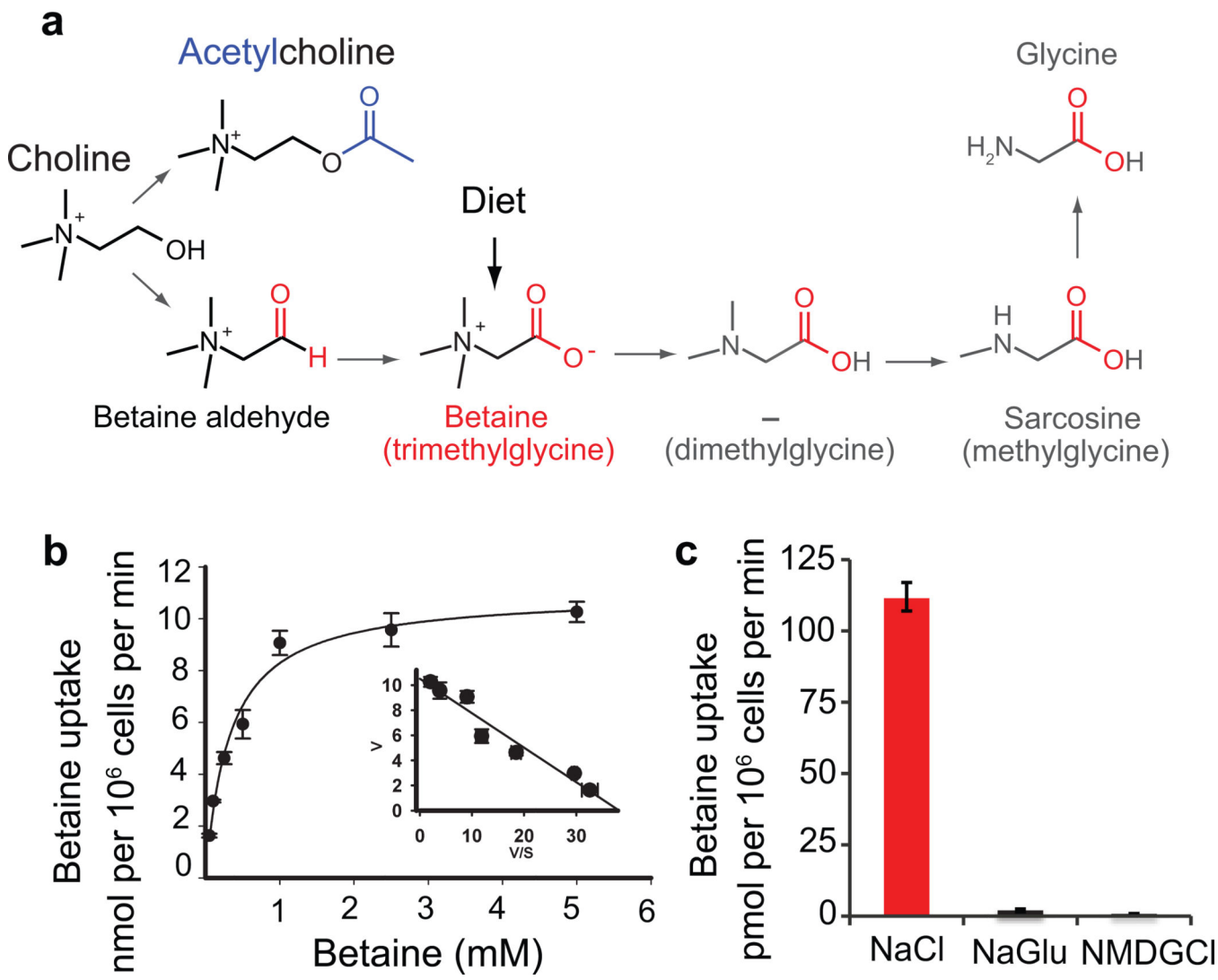

Figure 2. SNF-3 is a sodium chloride-dependent betaine transporter

(**a**) Betaine synthesis pathway. Betaine (*N*, *N*, *N*-trimethylglycine) is either acquired via diet or generated in two steps by oxidation of choline. (**b**) Saturation curve of betaine uptake by SNF-3 in HRPE cells. Error bars represent mean ± s.e.m. Each experiment was performed in triplicate. Inset: Eadie-Hofstee conversion of the same saturation data (v/s): [betaine uptake velocity (v) versus betaine uptake velocity/betaine concentration (v/s)]. Km was calculated using the Eadie-Hofstee equation. (**c**) SNF-3-mediated uptake of betaine is dependent on Na^+ and Cl^- ions. HRPE cells were incubated with 2.5 μM betaine for 15 minutes in assay buffer containing either NaCl, NaGlu or NMDGCl. Gluconate replaced chloride ions (NaGlu), and sodium ions were replaced by N-methyl-D-glucamine (NMDGCl). Error bars represent mean ± s.e.m. Each experiment was performed in triplicate.

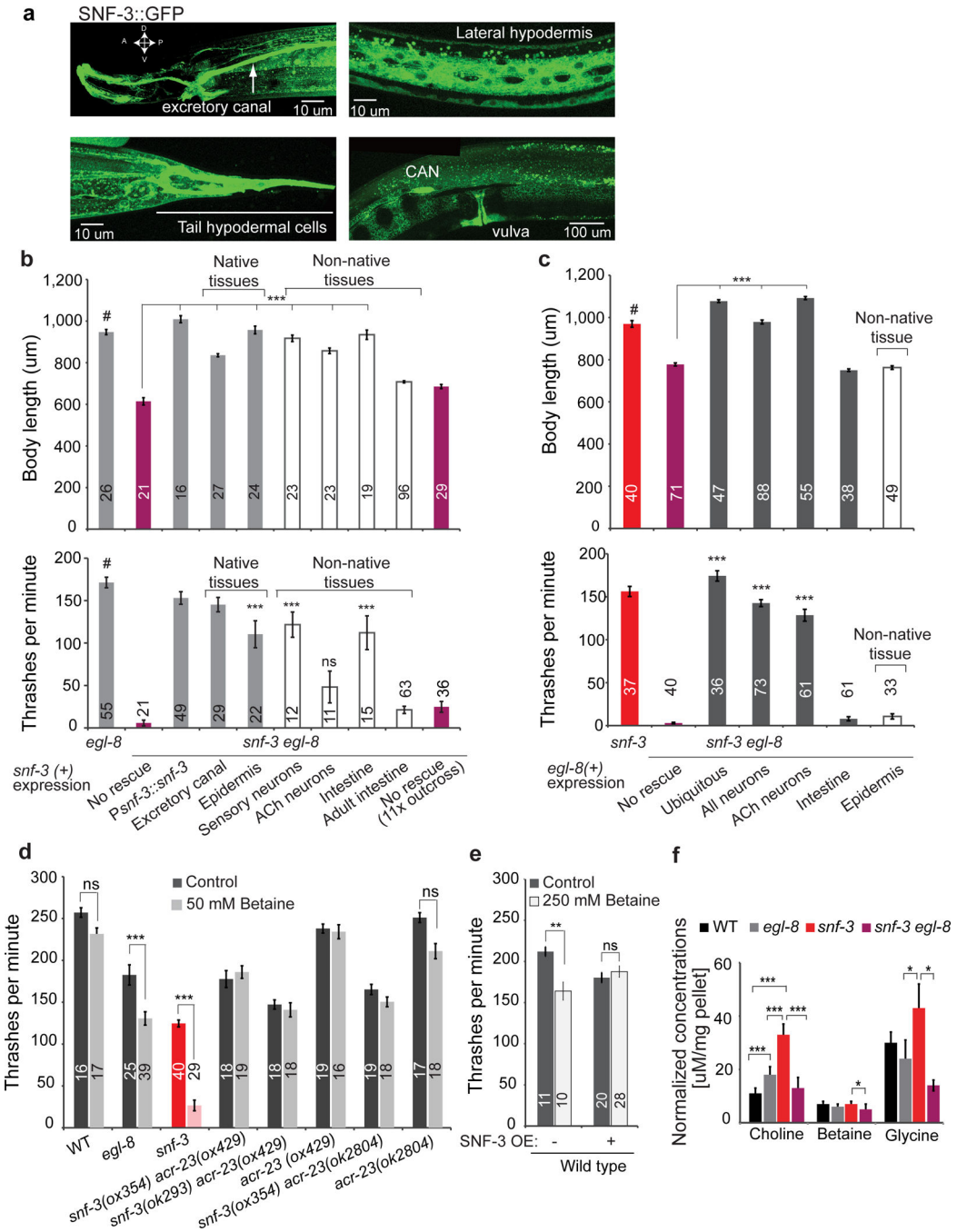

Figure 3. SNF-3 is required for betaine clearance

(**a**) Expression pattern of SNF-3::GFP. Images show the head, tail, lateral midbody and vulva region of a transgenic hermaphrodite expressing GFP fused to genomic SNF-3 (P*snf-3:: SNF-3- GFP::snf-3* utr). All images are adult hermaphrodites; anterior is to the left. (**b**) *snf-3* tissue-specific rescue of the hypercontracted (above) and locomotion (below) phenotype. Above, expression of SNF-3 cDNA in excretory canal (P*glt-3*), skin (P*pdi-2*), intestine (P*vha-6*), chemosensory neurons (P*odr-4*), or acetylcholine neurons (P*unc-17*) rescues the body morphology of *snf-3 egl-8* double mutants to normal *(egl-8* phenotype).

Expression in the adult intestine (P*vit-2*) did not rescue the phenotypes. The error bars represent the mean body length ± s.e.m. *** $p< 0.001$ compared to the *snf-3 egl-8* double mutants. The differences between the *egl-8* control and rescue of the *snf-3 egl-8* double mutant by expression of *snf-3(+)* in the excretory canal (*p=0.0088*) or in the acetylcholine motor neurons (*p=0.0031*) are statistically significant. Below, for the locomotion phenotype, the differences between *egl-8* control and rescue in the skin (*p=0.0003*) and intestine (*p=0.0048*) rescue are statistically significant. Expression of SNF-3 in the acetylcholine motor neurons did not rescue *snf-3 egl-8* locomotory defects ($p = 0.3702$), possibly because SNF-3 activity is electrogenic and interferes with motor neuron function. ns means not statistically significant. 'Native tissues' are cells that express the *snf-3* gene; 'non-native tissues' are cells in which *snf-3* gene expression was not detected. 11X outcrossed *snf-3 egl-8* is EG7513. The error bars represent thrashes ± s.e.m. *** $p< 0.001$ compared to the *snf-3 egl-8* double mutants. The number of animals tested is shown inside each bar. (**c**) Tissue-specific rescue of the *egl-8* hypercontracted (top) and locomotion (bottom) phenotypes. *egl-8* cDNA was expressed in all cells (P*dpy-30*), neurons (P*rab-3*), acetylcholine neurons (P*unc-17*), intestine (P*vha-6*), or epidermis (P*dpy-7*). Expression of EGL-8 in acetylcholine neurons (P*unc-17*) generates transgenic animals that are long and loopy-coilers. The number of animals tested is shown inside each bar. The error bars represent the means ± s.e.m. *** $p< 0.001$. Statistical significance was determined using one-way ANOVA followed by Tukey post-hoc comparisons. (**d**) Exogenous betaine slows locomotion. (**e**) Overexpression of SNF-3 confers resistance to excess betaine. For panels d and e the number of animals tested is shown inside each bar. The error bars represent the means ± s.e.m. Statistical significance was determined using one-way ANOVA followed by Tukey post-hoc comparisons. *** $p< 0.001$, ** $p< 0.01$, ns (not significant) $p > 0.05$. (**f**) Average concentrations of total betaine in whole animals. These metabolites were identified using Proton NMR spectroscopy. Statistical significance was determined using a one-way ANOVA on each metabolite with Bonferroni correction. $n= 8000$ animals per strain. ns, $p >0.05$, * $p< 0.05$, ** $p< 0.01$, *** $p< 0.001$. Alleles are *egl-8(sa47)* and *snf-3(ox354)*, unless indicated otherwise.

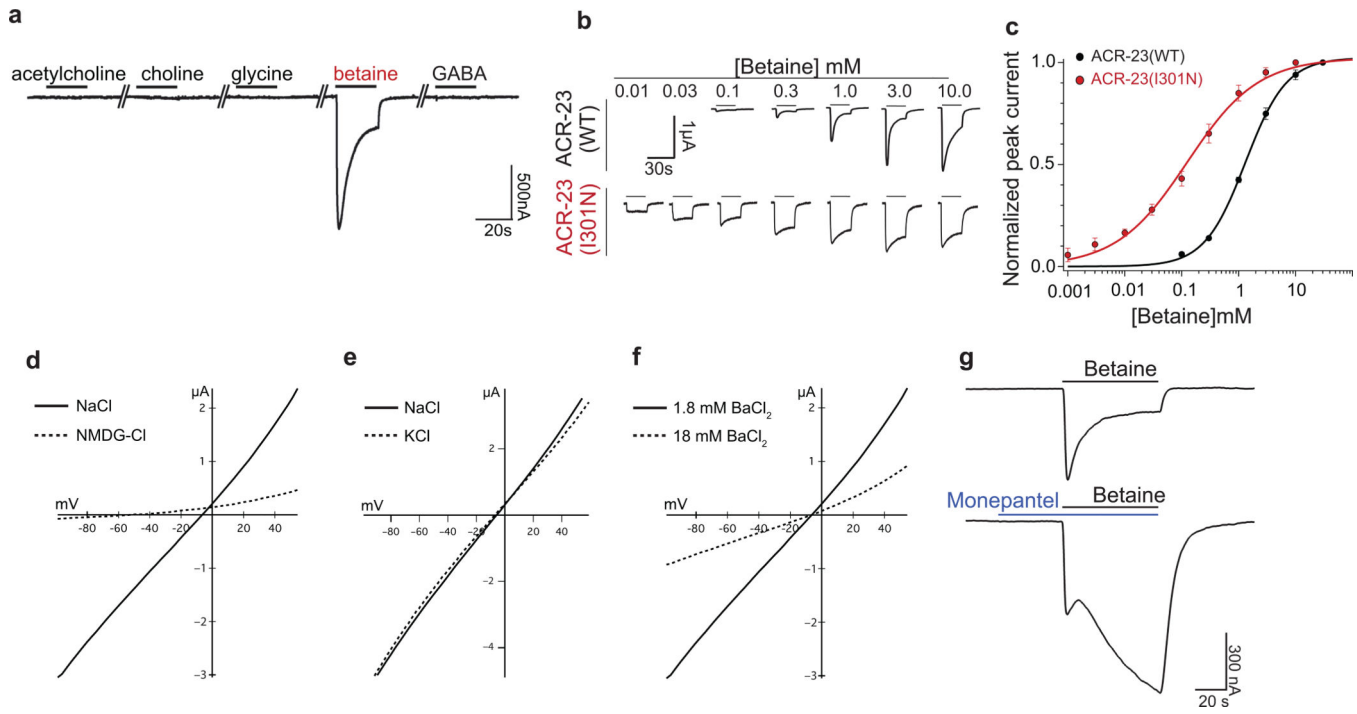

Figure 4. ACR-23 is a betaine-activated ion channel

(**a**) *Xenopus laevis* oocytes expressing ACR-23 respond to a 20 s pulse of 1mM betaine, but not 1mM acetylcholine, choline, glycine, or GABA. The mean betaine-evoked response = 1.3 ± 0.13 μA for oocytes injected with 0.1 ng cRNA (n = 9 oocytes). (**b**) Representative betaine-evoked currents from oocytes expressing ACR-23 or ACR-23(I301N) stimulated with the indicated betaine concentration. (**c**) Betaine sensitivity of the wild-type ACR-23 channel (black line, n = 6 oocytes) and ACR-23(I301N) gain-of-function channel (red line, n = 5). EC_{50} is 1.4 mM for the wild type and 166 μM for ACR-23(I301N) (p = 0.0017). Error bars are means ± s.e.m. Statistical significance was determined using two-tailed unpaired Student's t-test with Welch's correction. (**d,e,f**) ACR-23 is a monovalent cation channel. Insets indicate predicted ion flux under physiological conditions. (**d**) ACR-23 is permeable to sodium. Representative I-V curves in modified Ringer's solution containing Na^+ (n = 9) or NMDG (n = 8). (**e**) ACR-23 is potassium permeable. Representative I-V curves in modified Ringer's solution containing Na^+ (n = 7) or K^+ (n = 7). (**f**) ACR-23 is not permeable to the divalent cation Ba^{2+}. The reversal potential of betaine-evoked currents was not altered when extracellular Ba^{2+} concentration was increased 10-fold (n = 9). (**g**) Monepantel allosterically modulates ACR-23. A representative trace shows current induced by 1mM betaine in the absence (above) or presence (below) of 300 pM monepantel in oocytes expressing ACR-23 (n = 11).

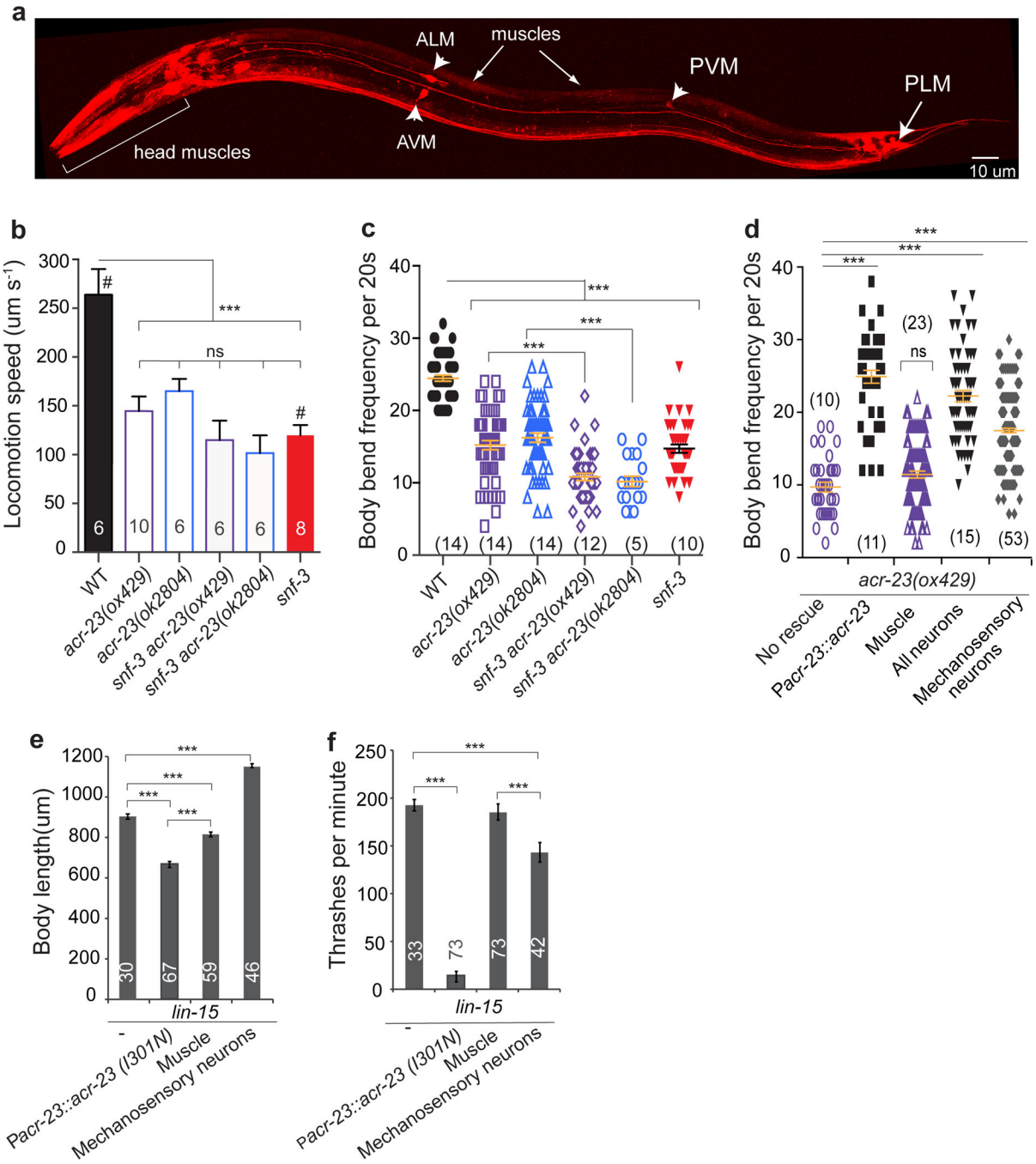

Figure 5. ACR-23 is required for sustained locomotion

(**a**) ACR-23 expression pattern. A transgenic hermaphrodite expressing mCherry driven by the *acr-23* promoter (P*acr-23::mCherry::let-858utr*). The strongest expression in the adult is in the mechanosensory neurons ALM, PLM, AVM and PVM (arrow heads) and head muscles (bracket). Expression is also seen in interneurons and body muscle. (**b**) Locomotion speed over a 5-minute period on an agar plate without food. Speed was determined using an automated worm tracking system. #, data from Fig. 1d. *** $p< 0.001$ ns, not significant ($p>0.05$). (**c**) Rate of body bends of animals on an agar plate. Each animal was tested 4 times

in the absence of food. *** $p< 0.001$. The number of animals tested is shown at the bottom of each column. The error bars represent the means ± s.e.m. (**d**) Neuronal expression rescues *acr-23* crawling defects. *** $p< 0.001$. The error bars represent the means ± s.e.m. The number of animals tested is shown at the bottom of each column. Each animal was tested 4 times in the absence of food. ns, not significant relative to no rescue. (**e,f**) ACR-23 activation reproduces *snf-3; egl-8* double mutant phenotypes. Quantification of the hypercontracted (**e**), and locomotion (**f**) phenotypes. *** $p< 0.001$. The number of animals tested is shown inside each bar. The error bars represent the means ± s.e.m. Statistical significance was determined using one-way ANOVA followed by Tukey post-hoc comparisons.